

Light scattering simulation by oblate disc spheres using the null field method with discrete sources located in the complex plane

JENS HELLMERS*[†], THOMAS WRIEDT[‡] and ADRIAN DOICU[§]

[†]Universität Bremen, Badgasteiner Str. 3, 28359 Bremen, Germany

[‡]Institut für Werkstofftechnik, Badgasteiner Str. 3, 28359 Bremen, Germany

[§]Remote Sensing Technology Institute, Oberpfaffenhofen,
82234 Wessling, Germany

(Received 10 March 2005)

The T-matrix method, which is also known as the null field method (NFM) or extended boundary condition method (EBCM), has established itself as a well known and highly regarded method for calculating light scattering by non-spherical particles. Its biggest advantage is the possibility to obtain all information about the scattering characteristics of the particle and to store it into one matrix. This enables one to do additional investigations with low efforts. Unfortunately the standard NFM fails to converge for particles with extremely non-spherical particle shapes, like long cylinders or coin-like flat cylinders. In this paper we investigate light scattering by finite particles in the form of an oblate disc sphere, which can be described as flat cylinders with a rounded edge. We use an advanced form of the T-matrix method—the null field method with discrete sources (NFM-DS). By presenting light scattering results we would like to demonstrate the potential this advanced NFM-DS offers. It allows one to calculate particle shapes with aspect ratios (relation between radius and thickness of the particle) up to 100:1 and size parameters (relation between radius and wavelength) up to 30.

1. Introduction

Over the years several approaches for simulation of light scattering by non-spherical particles have been developed. A good overview about these methods has been published by Wriedt and co-worker [1, 2] and Kahnert [3]. All these theories have advantages and disadvantages with regard to the topic of investigation; there is no general theory which would be capable of solving any problem which is of interest.

One well-known method is the T-matrix or null field method (NFM), which was developed by Waterman [4, 5]. It is based on an expansion of the incident, transmitted and the scattered field into a series of spherical vector wave functions (SVWF). For the conventional T-matrix method fast computer codes are easily available [6–8]. The biggest advantage and main characteristic of the NFM is that

*Corresponding author. Email: hellmers@iwt.uni-bremen.de

it enables one to calculate the T-matrix, in which all information of the scattering characteristics of the particle is stored. Once the T-matrix is known, additional investigations, e.g. like orientational averaging, scattering of particle clusters or particles with inclusions, can be done with low computational efforts. Unfortunately this method has stability problems with particles of extreme, non-spherical geometries, where it fails to converge.

In this paper we use an advanced form of the NFM—the null field method with discrete sources (NFM-DS)—as developed by Doicu and Wriedt [9–11] to cope with this limitations. We investigate the scattering characteristics of particles in the form of an oblate disc sphere. Such a particle can be described best as a very flat cylinder where the small side is rounded.

These kind of flat particles are of interest for example in the photochemical industry as they are the base for newly developed photo films (T-grains) or for the production of porcelain (kaolins).

To cope with the limitations of the conventional NFM and to enable light scattering calculations for non-spherical particles a number of modifications to this method have been suggested. This includes improved numerical methods [12], formal modifications of the single spherical coordinate-based NFM [13], different choices of basis functions [14], and the application of spheroidal coordinate formalism [15].

Here we use discrete sources located in the complex plane [9] where the approximate solution of the scattering problem is gained by considering the set of the tangential components of the lowest-order multipoles with different origins as a complete system of functions on the particle surface. The use of multipole sources located in the complex plane has advantages when analysing axisymmetric obstacles because for multipoles situated on the symmetry axis of the scatterer the equations become uncoupled, permitting a separate solution for each azimuthal mode. Originally Eremin and co-workers [16, 17] proved the usefulness of this approach together with the discrete sources method (DSM).

The NFM-DS with a matrix formulation including Hankel functions of low orders leads to better conditioned systems of equations compared to that obtained in the classical version of the NFM. The stability also increases because multiple origins are better suited to model the boundary geometry of highly elongated, prolated or oblated particles.

In this paper we investigate light scattering by oblate disc spheres. For the purpose of validation we compare the results we get by the NFM-DS with multipole sources in the complex plane with those we get from DSM.

For the NFM-DS we use a program developed by Doicu; the DSM results are gained by the work of Eremina and co-workers [18, 19].

2. Theory

The usual process of calculating the propagation of harmonic electromagnetic oscillations in the presence of local scatterers is done by solving the system of Maxwell equations by taking into account the radiation condition at infinity and the boundary conditions at the particle surface.

As we would like to prove the effectiveness of the NFM with multipole sources located in the complex plane, a set of tangential components of the lowest-order multipoles with different origins is considered as a complete system of functions on the particle surface.

Given is a three-dimensional space Ω consisting of the union of a closed surface S , its interior Ω_i and its exterior Ω_s . Then a point O within Ω_i is chosen to be the origin of a Cartesian coordinate system O_{xyz} . An arbitrary point in Ω is denoted by the position vector \mathbf{r} , while an arbitrary point on S is given by \mathbf{r}' . We denote by k_t the wave number of the region Ω_t , where $k_t = k(\varepsilon_t \mu_t)^{1/2}$, $t = s, i$ and $k = \omega/c$.

The mathematical formulation of the scattering problem of an incident field $(\bar{\mathbf{E}}_0, \mathbf{H}_0)$ by a homogeneous dielectric object with surface S consists of Maxwell's equations

$$\nabla \times \mathbf{E}_t = jk\mu_t \mathbf{H}_t, \quad \nabla \times \mathbf{H}_t = -jk\varepsilon_t \mathbf{E}_t \quad \text{in } \Omega_t,$$

where $t = s, i$, the boundary conditions on the particle surface

$$\mathbf{n} \times (\mathbf{E}_0 + \mathbf{E}_s - \mathbf{E}_i) = 0, \quad \mathbf{n} \times (\mathbf{H}_0 + \mathbf{H}_s - \mathbf{H}_i) = 0$$

on S where \mathbf{n} is the outward unit normal to S , $\varepsilon_s, \mu_s > 0$, and the radiation condition for $(\mathbf{E}_s, \mathbf{H}_s)$ uniformly over all possible radial directions.

Now the scattering object is replaced by a set of surface currents \mathbf{e} and \mathbf{h} over the surface S , so that in the exterior region the sources and fields are exactly the same as those existing in the original scattering problem while they are zero in the interior region.

The total electric field outside the scatterer $\mathbf{E}(\mathbf{r})$ is given by

$$\begin{aligned} \mathbf{E}(\mathbf{r}) = & \mathbf{E}_0(\mathbf{r}) + \nabla \times \int_S \mathbf{e}_i(\mathbf{r}') \cdot \mathbf{G}(k_S |\mathbf{r} - \mathbf{r}'|) dS \\ & - \nabla \times \nabla \times \int_S \frac{1}{jk\varepsilon_S} \mathbf{h}_i(\mathbf{r}') \cdot \mathbf{G}(k_S |\mathbf{r} - \mathbf{r}'|) dS \end{aligned} \quad (1)$$

for $\mathbf{r} \in \Omega_s$. Here $\mathbf{G}(k_S |\mathbf{r} - \mathbf{r}'|)$ is the Green's dyadic for the unbounded space; the null-field condition is $\mathbf{E}(\mathbf{r}) = 0$ for $\mathbf{r} \in \Omega_i$.

For the modified version of the single spherical coordinate-based NFM using multiple origins, a rigid translation z_p of the original coordinate system along the z axis is considered first. Here O_p denotes the origin of the new coordinate system, so that $\mathbf{r}_p = \mathbf{r} - z_p \mathbf{e}_3$. \mathbf{e}_i is the Cartesian system basis. Then the total electric field in the translated coordinate system O_p is expanded in terms of SVWF of the first kind $\mathbf{M}_{mn}^1(k_S \mathbf{r}_p)$ and $\mathbf{N}_{mn}^1(k_S \mathbf{r}_p)$, i.e.

$$\begin{aligned} \mathbf{E}(\mathbf{r}_p + z_p \mathbf{e}_3) = & \sum_{m \in \mathbb{Z}} \sum_{n \geq \max(1, |m|)} D_{mn} [a_{mn}^{(p)} (\mathbf{e}_i - \mathbf{e}_0, \mathbf{h}_i - \mathbf{h}_0)] \\ & \times \mathbf{M}_{mn}^1(k_S \mathbf{r}_p) + b_{mn}^{(p)} (\mathbf{e}_i - \mathbf{e}_0, \mathbf{h}_i - \mathbf{h}_0) \cdot \mathbf{N}_{mn}^1(k_S \mathbf{r}_p), \end{aligned} \quad (2)$$

where D_{mn} is a normalization constant and $\mathbf{e}_0 = \mathbf{n} \times \mathbf{E}_0$, $\mathbf{h}_0 = \mathbf{n} \times \mathbf{H}_0$.

The expansion coefficients $a_{mn}^{(p)}(\mathbf{e}, \mathbf{h})$ and $b_{mn}^{(p)}(\mathbf{e}, \mathbf{h})$ are expressed as surface integrals and are given by

$$\begin{aligned} a_{mn}^{(p)} &= \frac{ik_S^2}{\pi} \int_S \left[\mathbf{e} \cdot \mathbf{M}_{mn}^{(2)}(k_S \mathbf{r}'_p) + j \left(\frac{\mu_S}{\varepsilon_S} \right)^{1/2} \mathbf{h} \cdot \mathbf{N}_{mn}^{(2)}(k_S \mathbf{r}'_p) \right] dS, \\ b_{mn}^{(p)} &= \frac{ik_S^2}{\pi} \int_S \left[\mathbf{e} \cdot \mathbf{N}_{mn}^{(2)}(k_S \mathbf{r}'_p) + j \left(\frac{\mu_S}{\varepsilon_S} \right)^{1/2} \mathbf{h} \cdot \mathbf{M}_{mn}^{(2)}(k_S \mathbf{r}'_p) \right] dS. \end{aligned} \quad (3)$$

Let the set $\{z_p\}_{p=\overline{1, \infty}} = \Gamma_z$, where $\Gamma_z \subset \Omega_i$ is a segment of the z axis. Then it follows

- (a) that the system of the tangential components of the lowest-order SVWF with multiple origins $\{\mathbf{n} \times \mathbf{M}_{m,|m|+l}^1(k_i \mathbf{r}'_p), \mathbf{n} \times \mathbf{N}_{m,|m|+l}^1(k_i \mathbf{r}'_p)\}_{m \in \mathbb{Z}, p=\overline{1, \infty}}$ is complete on S and
- (b) that the infinite set of integral equations:

$$a_{m,|m|+l}^{(p)}(\mathbf{e}, \mathbf{h}) = 0 \quad \text{and} \quad b_{m,|m|+l}^{(p)}(\mathbf{e}, \mathbf{h}) = 0, \quad m \in \mathbb{Z}, \quad p = \overline{1, \infty}$$

assure the null-field condition for the total electric field within the enclosed volume, i.e. $\mathbf{E}(\mathbf{r}) = 0$ for $\mathbf{r} \in \Omega_i$. Here l is a fixed index given by $l = 1$ if $m = 0$ and $l = 0$ otherwise. The demonstration of the above results makes use of the vector addition theorem for SVWF under a translation of the coordinate origin.

The amplitude of the surface currents can be approximated in the mean-square norm by

$$\begin{aligned} \begin{pmatrix} \mathbf{e}_i^{\hat{N}} \\ \mathbf{h}_i^{\hat{N}} \end{pmatrix} &= \sum_{m=-M}^M \sum_{p=1}^N \alpha_{mp} \begin{pmatrix} \mathbf{n} \times \mathbf{M}_{m,|m|+l}^1(k_i \mathbf{r}'_p) \\ -j(\epsilon_i/\mu_i)^{1/2} (\mathbf{n} \times \mathbf{N}_{m,|m|+l}^1(k_i \mathbf{r}'_p)) \end{pmatrix} \\ &+ \beta_{mp} \begin{pmatrix} \mathbf{n} \times \mathbf{N}_{m,|m|+l}^1(k_i \mathbf{r}'_p) \\ -j(\epsilon_i/\mu_i)^{1/2} (\mathbf{n} \times \mathbf{M}_{m,|m|+l}^1(k_i \mathbf{r}'_p)) \end{pmatrix} \end{aligned} \quad (4)$$

and the amplitudes of the surface currents can be obtained as a solution of the truncated system of integral equations

$$\begin{aligned} a_{m,|m|+l}^{(p)}(\mathbf{e}_i^{\hat{N}} - \mathbf{e}_0, \mathbf{h}_i^{\hat{N}} - \mathbf{h}_0) &= 0, \\ b_{m,|m|+l}^{(p)}(\mathbf{e}_i^{\hat{N}} - \mathbf{e}_0, \mathbf{h}_i^{\hat{N}} - \mathbf{h}_0) &= 0, \quad m = \overline{-M, M}, \quad p = \overline{1, N} \end{aligned} \quad (5)$$

with \hat{N} as a complex index incorporating M and N .

Now, if the sequences $(\mathbf{e}_i^{\hat{N}}, \mathbf{h}_i^{\hat{N}})$ as solutions of the above scheme converge in the mean-square norm on S at $(\mathbf{e}_i, \mathbf{h}_i)$, then $(\mathbf{e}_i, \mathbf{h}_i)$ represent the unique surface currents of the scattering problem.

The approximate solution of the scattered field can be formally written as

$$\begin{aligned} \mathbf{E}_s^{\hat{N}}(\mathbf{r}) &= \nabla \times \int_S \mathbf{e}_i^{\hat{N}} \cdot \mathbf{G}(k_s|\mathbf{r} - \mathbf{r}'|) dS \\ &\quad - \nabla \times \nabla \times \int_S \frac{1}{jk\varepsilon_s} \mathbf{h}_i^{\hat{N}} \cdot \mathbf{G}(k_s|\mathbf{r} - \mathbf{r}'|) dS, \quad \mathbf{r} \in \Omega_s. \end{aligned} \quad (6)$$

This presentation concentrates on obtaining an approximate solution on the surface S . In a T-matrix scheme one expands the scattered field outside a circumscribed sphere in terms of SVWF, truncates this expansion at the index \hat{N} and computes the transition matrix which relates the scattered field coefficients to the incident field coefficients. This is fully outlined by Doicu *et al.* [11] and by Doicu and Wriedt [20]. Once the internal surface currents are determined, a formal solution of the scattered field can be constructed with the same form as (6).

The far-field vector amplitude $\mathbf{F}_s^{\hat{N}}(\theta, \varphi)$ of the scattered field, which allows one to compute energy characteristics, is calculated from

$$\mathbf{F}_s^{\hat{N}}(\theta, \varphi) = \lim_{r \rightarrow \infty} \mathbf{E}_s^{\hat{N}}(\mathbf{r}) \cdot r \exp(-jk_s r) \quad (7)$$

and the differential scattering cross-section (DSCS) from

$$\sigma_d^{\hat{N}} = \left| \mathbf{F}_s^{\hat{N}} \right|^2. \quad (8)$$

Now we take an axially symmetrical scatterer with the z axis as the symmetry axis of the particle. It is possible to reduce the problem of surface approximation to a sequence of one-dimensional problems relative to Fourier harmonics of the surface currents by using a system of multipoles distributed along the scatterer's axis of revolution and by expanding the external excitation in Fourier series. The approximation of the field on the surface S simplifies to the approximation of its Fourier harmonics on the generatrix L of the surface of revolution S . So multipoles situated on the axis of revolution adequately describe the particle geometry for prolate scatterers. But obviously this arrangement is not suitable for oblate scatterers. Eremin and co-workers introduced the idea of using a complex plane along the source coordinate z_p to handle this problem [16, 17].

Therefore we take the half-plane $\varphi = \text{const}$: $\Phi = \{(\rho, z) \mid \rho \geq 0, z \in \Re\}$ and define the complex plane $\hat{\Phi} = \{\hat{z} = (\text{Re}(\hat{z}), \text{Im}(\hat{z})) \mid \text{Re}(\hat{z}), \text{Im}(\hat{z}) \in \Re\}$ in such a way that the real axis $\text{Re}(\hat{z})$ coincides with the z axis. The spherical harmonics can be expressed

in terms of the coordinates of the source point $\hat{M}(\hat{z}) \in \hat{\Phi}$ and the observation point $M(\rho, z) \in \Phi$ by using the analytic continuation procedure

$$\begin{aligned} \mathbf{M}_{mn}^{1(3)}(k\mathbf{R}) &= z_n(kR) \left\{ im \frac{P_n^{m|}(\cos \hat{\theta})}{\sin \hat{\theta}} \left[\sin(\theta - \hat{\theta}) \mathbf{i}_r + \cos(\theta - \hat{\theta}) \mathbf{i}_\theta \right] \right. \\ &\quad \left. - \frac{dP_n^{m|}(\cos \hat{\theta})}{d\hat{\theta}} \mathbf{i}_\varphi \right\} \exp(im\varphi), \\ \mathbf{N}_{mn}^{1(3)}(k\mathbf{R}) &= \left\{ n(n+1) \frac{z_n(kR)}{kR} P_n^{m|}(\cos \hat{\theta}) \left[\cos(\theta - \hat{\theta}) \mathbf{i}_r - \sin(\theta - \hat{\theta}) \mathbf{i}_\theta \right] \right. \\ &\quad + \frac{[kR \cdot z_n(kR)]'}{kR} \frac{dP_n^{m|}(\cos \hat{\theta})}{d\hat{\theta}} \left[\sin(\theta - \hat{\theta}) \mathbf{i}_r + \cos(\theta - \hat{\theta}) \mathbf{i}_\theta \right] \\ &\quad \left. + \frac{[kR \cdot z_n(kR)]'}{kR} \cdot im \frac{P_n^{m|}(\cos \hat{\theta})}{\sin \hat{\theta}} \mathbf{i}_\varphi \right\} \exp(im\varphi), \end{aligned} \tag{9}$$

where $z_n(kR)$ stays for the spherical Bessel functions $j_n(kR)$ or the spherical Hankel functions $h_n^1(kR)$, $(\mathbf{i}_r, \mathbf{i}_\theta, \mathbf{i}_\varphi)$ are the unit vectors in spherical coordinates,

$$R^2 = \rho^2 + (z - \hat{z})^2, \quad \sin \hat{\theta} = \frac{\rho}{R}, \quad \cos \hat{\theta} = \frac{z - \hat{z}}{R}$$

and R is taken to be a branch corresponding to an arithmetical root on the real axis z .

Figure 1 shows how the boundary $L_{\hat{z}}$ of the domain $D_{\hat{z}} \in \hat{\Phi}$ coincides with the image of the curve L . The point $\hat{M}(\hat{z}) \in \hat{\Phi}$ is called the image of the point $M(\rho, z) \in \Phi$ if $R_{M\hat{M}}^2 = \rho^2 + (z - \hat{z})^2 = 0$, according to Eremin *et al.* [17]. So one can construct an approximate solution for the surface currents in the form of (4) and (5) if a set of

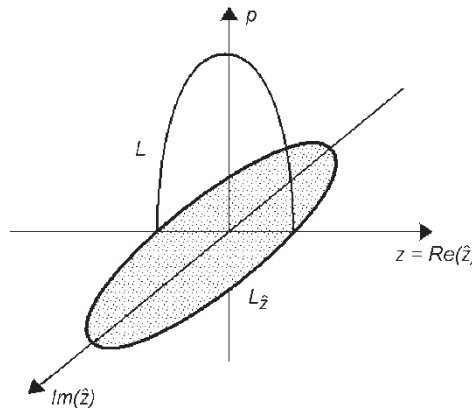


Figure 1. Sketch to illustrate the concept of the complex plane.

discrete poles $\{\hat{z}_p\}_{p=1,\infty} \subset D_{\hat{z}}$ has at least one limit point in $D_{\hat{z}}$, i.e. $\hat{z}_0 = \lim_{p \rightarrow \infty} \hat{z}_p$, $\hat{z}_0 \in D_{\hat{z}}$.

3. Description of the particle shape

In this paper we concentrate on light scattering by oblate disc spheres, which are coin-like flat cylinders with a rounded edge. So in the first step it is necessary to describe this kind of shape to get some input shape data for the numerical algorithm.

The basic and more easy shape is the flat cylinder (figure 2, left). It is described as follows:

$$\begin{aligned} r &= \frac{a}{\cos \theta}, & 0 \leq \theta < \arctan \frac{b}{a}, \\ r &= \frac{b}{\cos \theta}, & \arctan \frac{b}{a} \leq \theta < \arctan \frac{-a}{b}, \\ r &= \frac{-a}{\cos \theta}, & \arctan \frac{-a}{b} \leq \theta < \pi. \end{aligned} \tag{10}$$

Rotating this two-dimensional structure around the z axis leads to the wanted three-dimensional flat cylinder.

The rounded flat shape of an oblate disc sphere is described by adding a semicircle to the end of the flat cylinder described above (figure 2, right). By using the law of cosine—here $a^2 = y^2 + r_2^2 - 2yr_2 \cos(\pi - \theta)$ —and the aid of addition theorems one finds

$$\begin{aligned} r &= \frac{a}{\cos \theta}, & 0 \leq \theta < \arctan \frac{b}{a}, \\ r &= (b - a) \sin \theta + [a^2 - (b - a)^2 \cos^2 \theta]^{1/2}, & \arctan \frac{b}{a} \leq \theta < \arctan \frac{-a}{b}, \\ r &= \frac{-a}{\cos \theta}, & \arctan \frac{-a}{b} \leq \theta < \pi. \end{aligned} \tag{11}$$

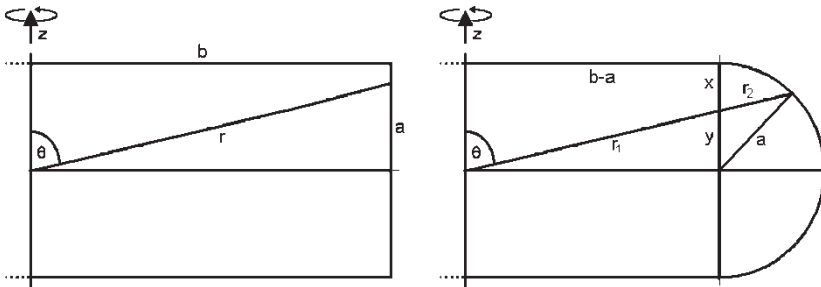


Figure 2. Sketch to illustrate the derivation of a mathematical description for a normal flat cylinder (left) and an oblated disc sphere (right) as used in this paper.

4. Convergence

To make sure that the scattering simulation results converge, the number of integration points (Nint) and the maximum expansion order (Nrank) have to be specified. In this case Nrank also defines the number of distributed sources and the dimension of the T-matrix.

For the convergence test over Nint the scattering problem is solved for a value Nint given by the user and Nint plus a small additional value dNint, which can also be configured freely. Testing convergence over Nrank is done by solving the scattering problem for a given Nrank and a lower value of Nrank which are also defined by the user. In both cases the normalized differential scattering cross-section will be checked at 20° increments if they adjoin to each other within a defined tolerance epsNint or epsNrank. If the calculated results converge within this tolerance at 80% of the scattering angles, then convergence is supposed to be achieved.

5. Scattering results

In the following we would like to present some computational results for light scattering by oblate disc spheres.

We varied the size parameter, which is given by $2\pi b/\lambda$ — b is the radius of the oblate disc sphere—and the aspect ratio, which means the ratio between the diameter of the particle in comparison to its height or thickness $2a$ (see also figure 2, right).

To get an impression of the quality of our results gained by the NFM with multipole sources in the complex plane we compare them with results computed from DSM. By doing so it is possible to investigate geometrical restrictions, i.e. the maximum size parameter and aspect ratio that gives convergent scattering results.

Additionally we also want to know how this method can be used in practical work and how it competes in this way compared with other methods. For this we take a closer look at simulation speed, the influence of double/quad precision and numerical stability.

5.1 General results—comparison with DSM

To demonstrate the validity of the NFM-DS we calculated the differential scattering cross-section (DSCS) for several different oblate disc spheres with different aspect ratios ranging from 20:1 to 100:1 and two different size parameters of 20 and 30. The refractive index of the particles is 1.5 and the plane wave is incident along the axis of symmetry of the disc sphere. These results were compared with those we get from the DSM [18, 19].

To give an impression of the investigated particle shapes figure 3 shows the corresponding profiles. The corresponding light scattering patterns for these particles are shown in figure 4.

All these results show very good accordance between NFM-DS and DSM with the exception of the result for the 80:1 aspect ratio. Here one can observe some

	size param.	aspect ratio
	20	20:1
	20	40:1
	30	60:1
	20	80:1
	30	100:1

Figure 3. Profiles of the simulated oblate disc spheres.

deviation of the DSCS for scattering angles of about 90° where the scattered intensity is low. This is the particle shape with the lowest thickness. It indicates that the thickness might be a limiting factor for getting satisfactory results for light scattering simulation.

In general it was found that the NFM with discrete sources in the complex plane is suitable to calculate oblate disc spheres up to size parameters of 30 and aspect ratios of 100:1. This is a remarkable improvement compared to the standard NFM. As with the conventional T-matrix method with the NFM-DS it is now possible to calculate and store the T-matrix which is describing the whole scattering process and to do further investigations with a low amount of computational expense.

5.2 Light scattering with different incident angles

With the NFM it is not only possible to simulate light scattering of an oblate disc sphere with the direction of the incident light parallel to the axis of symmetry. It is also possible to calculate light scattering results for any direction of incident light from precomputed T-matrices.

Next we would like to present some light scattering diagrams for an oblate disc sphere where the direction of the incident light is not parallel to the rotational axis and compare these results again with a result calculated from DSM.

Figure 5 shows light scattering diagrams for the same oblate disc sphere with an aspect ratio of 5:1 and a size parameter of 7.5 for greater incident angles θ between the axis of rotation and the incident light; $\theta = 0, 15, 30, 45, 60, 75$ and 90° . The refractive index is 1.5.

One can make several observations: for low incident angles θ between the direction of incident light and the rotational axis of the particle we get good congruence between NFM-DS and DSM light scattering results. This range goes from 0 to 45° . For greater angles the results get worse, but they still show the same tendency. An interesting fact is that only the perpendicular polarization shows

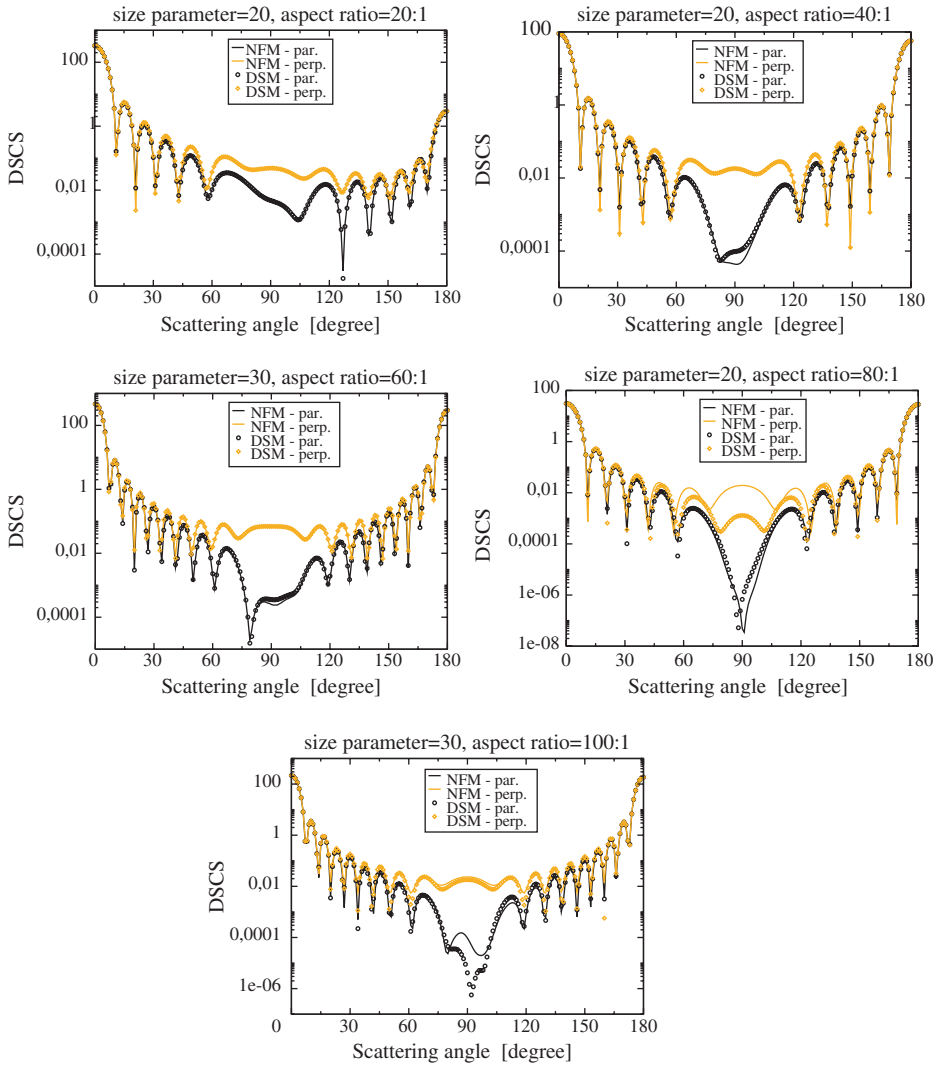


Figure 4. Comparison between NFM with discrete sources in the complex plane and DSM. Shown are the results for parallel and perpendicular DSCS for oblate disc spheres of different sizes and aspect ratios. The direction of incident light is parallel to the rotational axis, the refractive index is 1.5. Top left: size parameter=20, aspect ratio=20:1, $N_{\text{int}}=500$, $N_{\text{rank}}=27$. Top right: size parameter=20, aspect ratio=40:1, $N_{\text{int}}=2000$, $N_{\text{rank}}=32$. Middle left: size parameter=30, aspect ratio=60:1, $N_{\text{int}}=3000$, $N_{\text{rank}}=38$. Middle right: size parameter=20, aspect ratio=80:1, $N_{\text{int}}=5000$, $N_{\text{rank}}=32$. Bottom: size parameter=30, aspect ratio=100:1, $N_{\text{int}}=5000$, $N_{\text{rank}}=36$. (The colour version of this figure is included in the online version of the journal.)

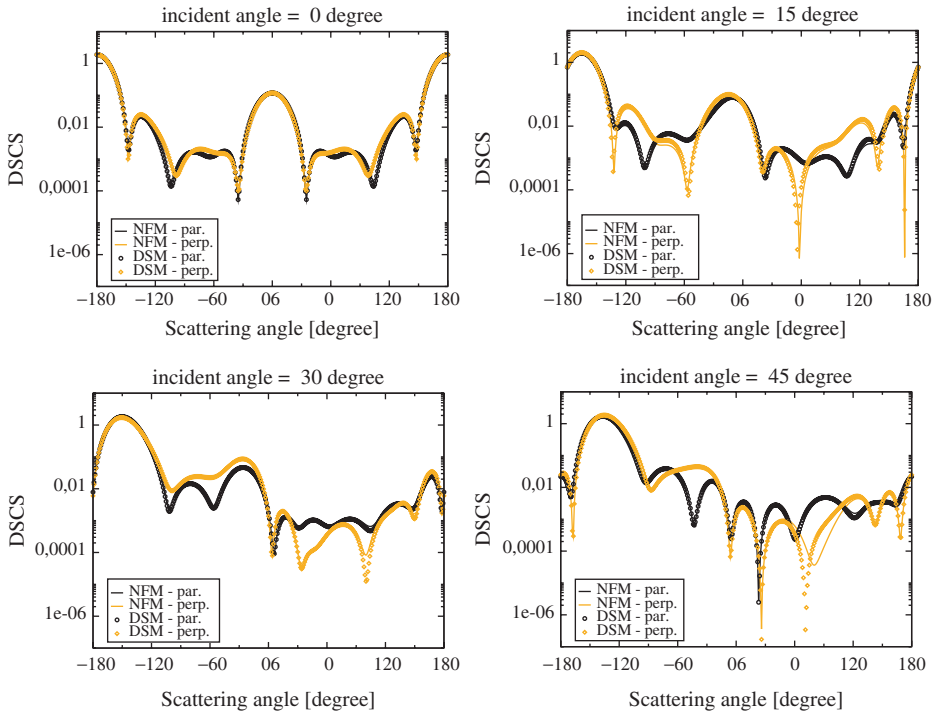


Figure 5. Comparison between NFM and DSM. Shown are the results for parallel and perpendicular DSCS for an oblate disc sphere with a size parameter of 7.5 and an aspect ratio of 5:1 for different angles θ between the axis of rotation and the incident light. θ was chosen from 0 to 90° in 15° steps. The refractive index is 1.5 for all calculations. $N_{\text{int}} = 500$, $N_{\text{rank}} = 18$. (The colour version of this figure is included in the online version of the journal.)

this behaviour; the graphs for the parallel polarization calculated by NFM-DS and DSM show congruence in every diagram. Again it is difficult to decide which method produces diverging results. One hint might be that the residual for the DSM based calculation showed different values for parallel and perpendicular polarization.

5.3 Light scattering results for disc spheres with the same size parameter, aspect ratio or volume

It is possible to classify oblate disc spheres by several attributes: size parameter, aspect ratio or volume. Here we would like to present light scattering results for oblate disc spheres where one attribute is kept constant while the others are varied. For all calculations the particles have a refractive index of 1.5 and the incident light is parallel to the rotational axis.

To estimate the influence of the aspect ratio we calculated scattering by oblate disc spheres with same size parameter and different aspect ratios. Figure 6 shows the light scattering diagrams for three oblate disc spheres with a constant size parameter of 10 and aspect ratios of 2:1, 5:1 and 10:1.

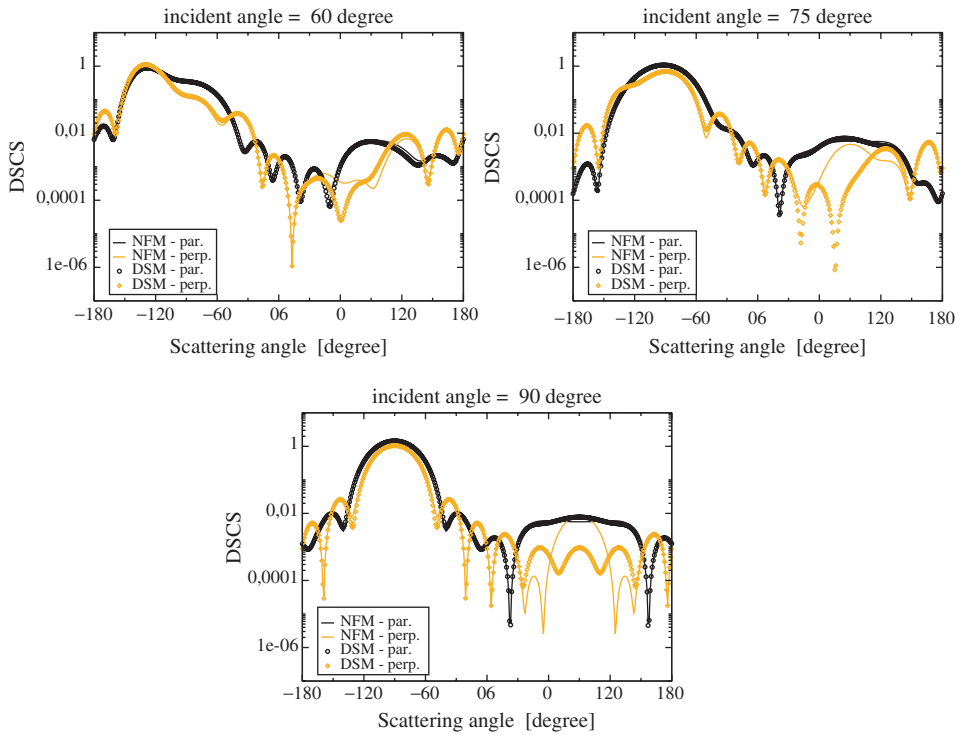


Figure 5. Continued. (The colour version of this figure is included in the online version of the journal.)

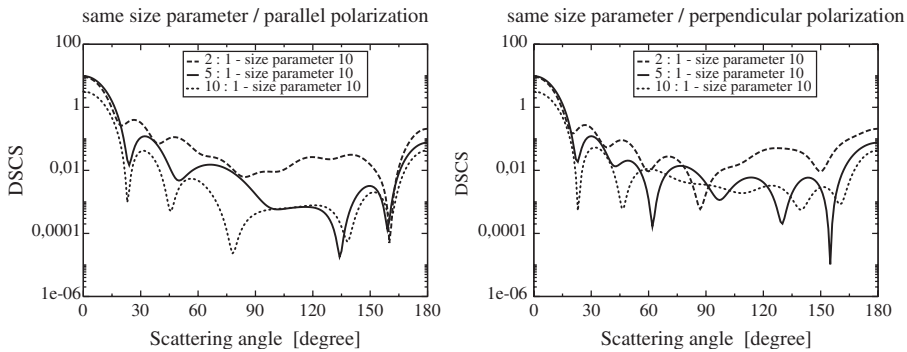


Figure 6. Light scattering diagrams for oblate disc spheres with a size parameter of 10 and three different aspect ratios. Left: parallel polarization, right: perpendicular polarization. The aspect ratios are 2:1, 5:1 and 10:1. The direction of incident light is parallel to the rotational axis, the refraction index is 1.5. For aspect ratio 2:1, $N_{int} = 1000$ and $N_{rank} = 22$. For aspect ratio 5:1, $N_{int} = 1000$ and $N_{rank} = 22$. For aspect ratio 10:1, $N_{int} = 1000$ and $N_{rank} = 21$.

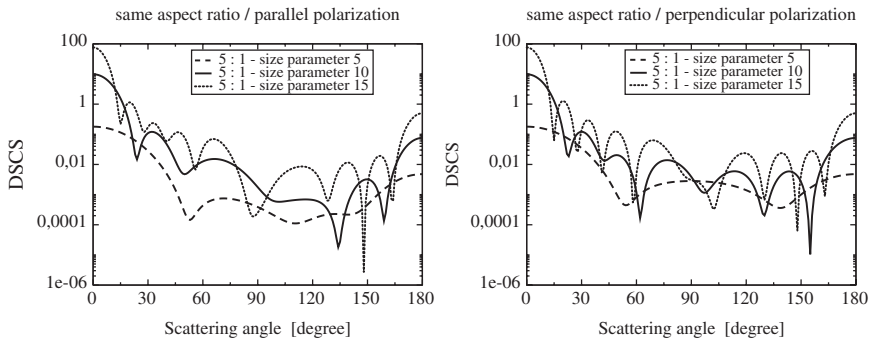


Figure 7. Light scattering diagrams for oblate disc spheres with an aspect ratio of 5:1 and three different size parameters. Left: parallel polarization, right: perpendicular polarization. The size parameters are 5, 10 and 15. The direction of incident light is parallel to the rotational axis, the refraction index is 1.5. Size parameter 5: $N_{int} = 1000$, $N_{rank} = 16$. Size parameter 10: $N_{int} = 1000$, $N_{rank} = 22$. Size parameter 15: $N_{int} = 1500$, $N_{rank} = 32$.

The most noticeable observation is the increasing overall scattering intensity the lower the aspect ratio gets. This is due to the increasing volume (this effect can be observed in figure 8, too). This is especially obvious for parallel polarization where the effect is much more distinct than for the perpendicular polarization.

In the next step we would like to present the scattering diagrams for three oblate disc spheres with the same aspect ratio and different size parameters. Figure 7 shows the light scattering diagrams for three oblate disc spheres with an aspect ratio of 5:1 and size parameters of 5, 10 and 15.

Keeping the aspect ratio constant and varying the size parameter has an influence mostly on the number of minima and maxima. As everybody would expect the number increases the larger the size parameter gets.

To complete these comparisons we investigated the light scattering by disc spheres with the same volume but different size parameters and aspect ratios. The volume of an oblate disc sphere can be calculated by the general formula for bodies with one rotational axis. In general this leads to

$$V = 2\pi \left(\frac{1}{2} hr^2 - rh^2 \left(\frac{1}{2} - \frac{1}{8} \pi \right) + h^3 \left(\frac{5}{24} - \frac{1}{16} \pi \right) \right) \quad (12)$$

where r is the radius of the disc sphere and h is the height or thickness. In this case $r = b$ and $h = 2a$ (see figure 2, right).

Figure 8 shows the light scattering diagrams for three oblate disc spheres with a volume of $1.15 \mu\text{m}^3$ and size parameters of 8, 10 and 12 which leads to aspect ratios of 2.3:1, 5:1 and 8.9:1 respectively.

The diagrams for equivolume oblate disc spheres show a mixture of both observations. As mentioned above the most obvious observation here is the fact that the overall scattering intensity keeps constant.

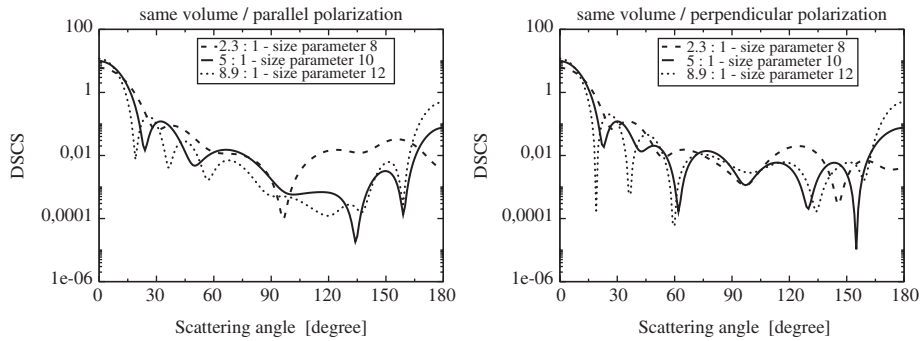


Figure 8. Light scattering diagrams for equivolume disc spheres with different size parameters and aspect ratios. Left: parallel polarization, right: perpendicular polarization. The volume is $1.15 \mu\text{m}^3$, the size parameters are 8, 10 and 12 with corresponding aspect ratios of 2.3:1, 5:1 and 8.9:1. The direction of incident light is parallel to the rotational axis, the refraction index is 1.5. For size parameter 8, aspect ratio 2.3:1, $N_{\text{int}} = 300$, $N_{\text{rank}} = 23$. For size parameter 10, aspect ratio 5:1, $N_{\text{int}} = 300$, $N_{\text{rank}} = 23$. For size parameter 12, aspect ratio 8.9:1, $N_{\text{int}} = 500$, $N_{\text{rank}} = 26$.

5.4 Influence of quad/double precision, different compilers on different computer systems and computational speed

All the NFM calculations presented so far were done with quad precision. Now one could get the idea of changing to double precision to save computational time. To check this we modified the program and compiled it for double precision accuracy. Unfortunately the results one gets then are completely useless and therefore not presented here. So quad precision is necessary for this kind of light scattering simulation.

As this proved to be some critical issue we then investigated the influence of different compilers on different computer systems.

Figure 9 shows the results for an oblate disc sphere with a size parameter of 30 and an aspect ratio of 4:1. Calculation was done on two different computer systems with two different compilers. The first one was the Compaq Fortran compiler running on a Compaq Alpha EV67 with 667 MHz CPU speed—this was the standard system for the simulations presented here. The second one was calculated on an Athlon PC 2200+ with the Fujitsu Lahey Fortran compiler running on a Windows environment.

The results we got are identical so there is no influence caused by the compiler or computer system used. Additionally it should be mentioned that the results for DSM—which leads to the same results as shown before—were calculated on a PC with the Compaq Fortran compiler on a Windows environment. This compiler works with double precision; in this case IMSL routines provide the program with the ability to work with higher precision numbers. So two different methods done on three different platforms with three different compilers lead to the same results.

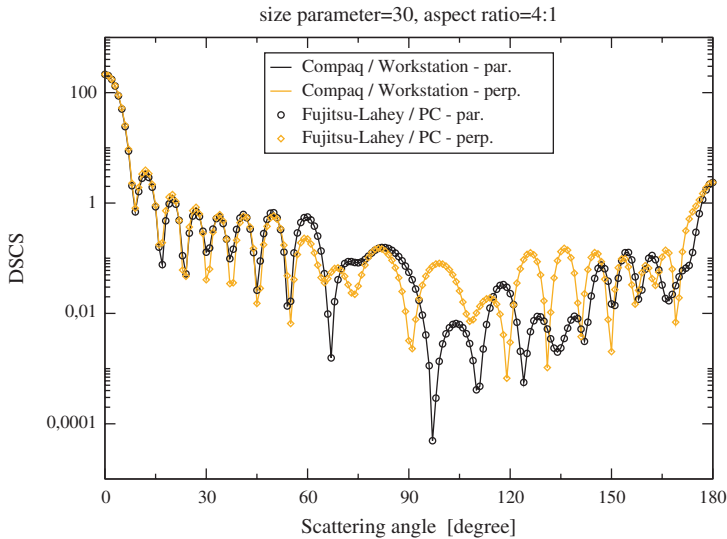


Figure 9. Results for the DSCS of an oblate disc sphere with a size parameter of 30 and an aspect ratio of 4:1—comparison between two different compilers for the same program based on the NFM with discrete sources in the complex plane. The direction of incident light is parallel to the rotational axis, the refraction index is 1.5. $N_{\text{int}} = 1000$, $N_{\text{rank}} = 32$. (The colour version of this figure is included in the online version of the journal.)

Another point of interest are the computational expenses. For this it is difficult to give a statement. The platforms used are too different regarding their architecture to allow one to compare the computational times which the different compiled programs needed. Also no special compiler options were used. In practice the workstation was much faster than the PC. The same can be said about a comparison of computational time for the NFM-DS and the DSM. Here another fact plays an even bigger role: to get reasonable NFM-DS results it is necessary to use ‘good’ parameters in the spherical vector wave functions series. Practice shows that the results one gets converge in a small area of parameters and then start to diverge if the development goes too far. Because of this the program used includes algorithms to check for convergence. This checking for convergence can be very time consuming while the scattering computation itself is very fast.

6. Summary

In this paper we intended to demonstrate that the extension of the conventional T-matrix method by using discrete sources, which are arranged in the complex plane, can overcome the biggest lack of this standard NFM as it enables one to calculate light scattering of extremely non-spherical particles. To demonstrate this we chose coin-like oblate disc spheres as objects of investigations.

By comparing with the results one gets from DSM it was shown that the NFM with discrete sources in the complex plane is suitable to calculate oblate disc spheres up to size parameters of 30 and aspect ratios of 100:1. This is a remarkable advancement compared to the conventional T-matrix method.

Additionally results for different classes of oblate disc spheres (some size parameter, same aspect ratio, same volume) and an investigation of the influence of the numerical precision and different compilers on the simulation process were presented.

Acknowledgment

We would like to acknowledge support of this work by Deutsche Forschungsgemeinschaft DFG.

References

- [1] T. Wriedt, Part. Part. Syst. Charact. **15** 67 (1998).
- [2] T. Wriedt and U. Comberg, J. Quant. Spectrosc. Radiat. Transfer **60** 411 (1998).
- [3] F.M. Kahnert, J. Quant. Spectrosc. Radiat. Transfer **79–80** 775 (2003).
- [4] P.C. Waterman, Proc. IEEE **53** 805 (1965).
- [5] P.C. Waterman, J. Acoust. Soc. Am. **45** 1417 (1969).
- [6] P.W. Barber and S.C. Hill, *Light Scattering by Particles: Computational Methods* (World Scientific, Singapore, 1990).
- [7] M.I. Mishchenko and L.D. Travis, J. Quant. Spectrosc. Radiat. Transfer **60** 309 (1998).
- [8] <http://www.t-matrix.de>
- [9] A. Doicu and T. Wriedt, Opt. Commun. **139** 85 (1997).
- [10] T. Wriedt and A. Doicu, J. Mod. Opt. **45** 199 (1998).
- [11] A. Doicu, Y. Eremin and T. Wriedt, *Acoustic and Electromagnetic Scattering Analysis using Discrete Sources* (Academic Press, San Diego, 2000).
- [12] P.C. Waterman, Phys. Rev. D **3** 825 (1971).
- [13] A. Boström, J. Acoust. Soc. Am. **76** 588 (1984).
- [14] R.H.T. Bates and D.J.N. Wall, Phil. Trans. R. Soc. Ser. A **287** 45 (1977).
- [15] R.H. Hackman, J. Acoust. Soc. Am. **75** 35 (1984).
- [16] Y.A. Eremin and A.G. Sveshinov, *The Discrete Sources Method in Electromagnetic Scattering Problems* (Moscow State University Publ. House, Moscow, 1992) (in Russian).
- [17] Y.A. Eremin, N.V. Orlov and V.I. Rozenberg, Comput. Phys. Commun. **79** 201 (1994).
- [18] E. Eremina and T. Wriedt, J. Quant. Spectrosc. Radiat. Transfer **89** 67 (2004).
- [19] E. Eremina, Y. Eremin and T. Wriedt, Opt. Commun. **244** 15 (2005).
- [20] A. Doicu and T. Wriedt, J. Opt. Am. A **16** 2539 (1999).